DYNAMIC MANAGEMENT OF THERMAL ENERGY IN MULTI-TEMPERATURE COLD CHAIN SUPPLY CHAIN AND ECONOMIC EVALUATION OF HEAT STORAGE TECHNOLOGY

by

Tianqi LI [a] ***and Xia HUA*** [b,c*]

[a] Faculty of Modern Agriculture, Dazhou Vocational and Technical College, Dazhou, China
[b] School of Economics and Management, Wenshan University, Wenshan, China
[c] Graduate School of Business, SEGi University, Kuala Lumpur, Malaysia

Original scientific paper
https://doi.org/10.2298/TSCI2506217L

This paper designs a dynamic management system for thermal energy in multi-temperature cold chains, constructs a monitoring system that includes sensor selection and lay-out, data acquisition and transmission, proposes a control strategy, and builds an intelligent platform. Through experimental simulation, in terms of temperature stability,co-ordinated control uses a coupling coefficient matrix to pre-compensate for adjacent zone interference, while paraffin's stable phase change (205 kJ/kg latent heat) maintains temperatures during fluctuations. This synergy achieves 28.3% savings and 1.1 ℃ max deviation. In terms of energy saving effect, the energy saving rate of the entire temperature zone combination reaches 28.3%, and the energy consumption per unit time in the door opening stage decreases by 33.3%. The heat storage performance test reveals that the efficiency of paraffin decreases by 3.2% after 50 cycles, with a constant temperature time of 6.2 hours for heat release. The study shows that the system can effectively improve temperature stability and reduce energy consumption.

Key words: *dynamic management of thermal energy, thermal storage evaluation, experimental simulation, multi-temperature zone cold chain, temperature stability*

Introduction

In the fields of fresh agricultural product circulation and biomedical transportation, the multi-temperature zone cold chain supply chain is the core link to ensure product quality, and its technological upgrade has become an urgent need for the industry's development. With the increasing demand for consumption and the standardized development of the pharmaceutical industry, the market for multi-temperature zone cold chains is growing [1]. Data show that in 2024, the scale of Chinese fresh cold chain market is expected to exceed 500 billion Yuan, and the scale of the pharmaceutical cold chain market will exceed 120 billion Yuan, with multi-temperature zone distribution business accounting for 35% and 42%, respectively. Compared to the traditional single-temperature zone cold chain, the multi-temperature zone system requires maintaining multiple differentiated temperature zones, such as freezing (–25 ℃ to –18 ℃), refrigeration (2-8 ℃), and constant temperature (10-15 ℃), which places higher requirements on the accuracy of thermal energy regulation [2]. A 2 ℃ deviation raises

* Corresponding author, e-mail: huaxiasummer@foxmail.com

fresh product loss by 5% (per cold chain studies), while our system's 1.1 ℃ max deviation cuts loss to <5%, matching developed country levels. The use of multi-temperature zone collaborative distribution can reduce logistics costs by 15%-20%. However, the product loss rate caused by unbalanced thermal energy management in existing technologies remains as high as 8% to 12%, which is significantly higher than the level of less than 5% in developed countries. The economic losses caused each year exceed 30 billion Yuan.

As a key technology for balancing energy consumption and temperature control accuracy across multiple temperature zones, dynamic thermal energy management centers on the precise distribution of thermal energy through real-time monitoring and intelligent control [3]. In current research, the traditional control method based on the PID algorithm has a response lag problem. Under the interference of drastic changes in external ambient temperature or frequent opening and closing of doors, the fluctuation range of the temperature zone often exceeds ±1.5 ℃, which cannot meet the strict temperature control requirements of high-end fresh food and biological preparations [4]. Although the integrated application of heat storage technology can alleviate this contradiction a certain extent and reduce temperature fluctuations, the compatibility evaluation of different materials (such as phase change materials and sensible heat materials) still lacks systematic data support [5]. For example, paraffin PCM offer advantages in heat storage density but have poor thermal conductivity. Water, as a sensible heat material, has a low cost but limited heat storage capacity.

Additionally, domestic and foreign research focuses on optimizing individual links, such as temperature control in transport vehicles or energy-saving transformations in cold storage facilities. However, research on the co-ordinated management of the entire heat flow chain remains insufficient [6]. In actual operation, the multi-temperature zone cold chain involves multiple links, including procurement, transportation, warehousing, and sales. The heat loss characteristics of each link are different, and there is a close relationship between them [7]. Optimizing a single link is difficult, as it does not lead to overall efficiency improvement. At the same time, existing research in experimental simulation primarily employs simplified models, which fail to accurately simulate the actual, complex cold chain environment, resulting in a low conversion rate of research results into practical applications.

This study focuses on the dynamic characteristics of thermal energy in multi-temperature zone cold chains. It constructs an integrated management system that includes distributed sensing, intelligent control, and data mining [8]. By building a 5 m³ simulation experimental platform, the operation scenarios of different temperature zone combinations (frozen + refrigerated, frozen + constant temperature, whole temperature zone) are simulated. Interference factors, such as external environmental temperature changes and the frequency of door opening and closing, are introduced to make the experimental conditions more closely resemble the actual situation [9]. In the experiment, the performance differences in heat storage efficiency, heat release rate, and other aspects of paraffin, water, and composite heat storage materials were compared. An improved co-ordinated control algorithm was used to verify the system's performance. The algorithm combines the advantages of fuzzy control and PID control to enhance the system's response speed and control accuracy [10]. The research results can provide technical references for energy-saving and consumption reduction in multi-temperature zone cold chains, helping the industry break through the development bottleneck of *high energy consumption-low precision* and promoting the development of China's cold chain industry in the direction of high efficiency, precision, and low carbon.

Design of thermal energy dynamic management system

Construction of thermal energy dynamic monitoring system

Selection and lay-out of sensors

Given the complex environment of a multi-temperature cold chain, the sensor must meet the temperature measurement range of –30-20 °C and the accuracy requirement of ±0.1 °C. A distributed lay-out solution is adopted, with 1 PT100 platinum resistance sensor installed every 5 m^2 in the freezing area (–25 °C to –18 °C), infrared temperature measurement sensors are used in the refrigeration area (2-8 °C), and temperature difference compensation sensors are added at the junction of the temperature zones [11]. The sensor lay-out density follows the spatial attenuation model:

$$N_i = S_i \mathrm{e}^{-k\Delta T_i} \rho \tag{1}$$

where N_i is the number of sensors in temperature zone i, S_i – the area of the zone, k – the attenuation coefficient (take 0.02 °C^{-1}), ΔT_i – the temperature difference between the temperature zone and the environment, and ρ – the cargo stacking density correction coefficient (0.8-1.2). Where ρ = 1.2 for dense cargo (*e.g.*, frozen meat) increases sensors by 20% *vs*. loose cargo (ρ = 0.8), ensuring coverage in heat-trapping areas, validated via thermal mapping.

Data acquisition and transmission technology

Time division multiplexing technology is used to realize multi-node data acquisition, and the sampling frequency, f_s, is dynamically adjusted according to the stability requirements of the temperature zone:

$$f_s = f_0 \left(1 + \alpha \sigma_T\right) \tag{2}$$

where f_0 is the base frequency (1 Hz), α – the sensitivity coefficient (taken as 0.5), and σ_T – the standard deviation of the temperature in the past five minutes. The transmission layer adopts the improved LoRa protocol, and the communication distance, d, satisfies:

$$d = d_0 \cdot 10^{-\gamma\left(\frac{d_0}{d_1}\right)} \tag{3}$$

where d_0 is the reference distance (100 m), γ – the path loss factor (taken as 2.3), and d_1 – the equivalent distance of the obstacle.

Dynamic control strategy of thermal energy

Temperature control method based on real-time data

An adaptive PID control model is established, and the dynamic correction formula of its proportional coefficient, K_p, is:

$$K_p\left(t\right) = K_{p0}\left[1 + \beta \tanh\left(\frac{\Delta T\left(t\right)}{\Delta T_0}\right)\right] \tag{4}$$

where K_{p0} is the initial proportional coefficient, β – the adjustment factor (0.3-0.7), $T(t)$ – the real-time temperature difference, and ΔT_0 – the reference temperature difference (2 °C). The calculation formula of cooling power, P_c, is:

$$P_c = P_{c0}\sqrt{\frac{\Delta T\left(t\right)}{\Delta T_{\mathrm{set}}}}\mathrm{e}^{-\lambda t} \tag{5}$$

where P_{p0} is the rated power, ΔT_{set} – the set temperature difference, and λ – the attenuation coefficient. The $\lambda = 0.01$ tuned via 50 trials: $\lambda = 0.02$ caused 1.5 °C spikes, $\lambda = 0.005$ wasted 15% energy. This value balances decay and stability.

Co-ordinated control mechanism of thermal energy between different temperature zones

The temperature zone coupling coefficient matrix, $C_{i,j}$, is constructed to characterize the thermal energy interference of temperature zone i to temperature zone j:

$$C_{i,j} = \frac{\kappa A_{i,j} \Delta T_{i,j}}{d_{i,j} R_{i,j}} \tag{6}$$

where κ is the thermal conductivity coefficient, $A_{i,j}$ – the adjacent area, $\Delta T_{i,j}$ – the temperature difference between the temperature zones, $d_{i,j}$ – the spacing distance, and $R_{i,j}$ – the thermal resistance of the insulation layer. The $R_{i,j} = 2.5$ m^2 K/W (polyurethane) and 5.0 (aerogel), measured via heat flux meter, ensuring accurate coupling calculations for different insulation types. Total energy consumption optimization objective function:

$$\min E_{\text{total}} = \sum_{i=1}^{n} E_i + \sum_{i \neq j} C_{i,j} E_i E_j \tag{7}$$

The constraint condition is that the temperature deviation of each temperature zone $|\Delta Ti| \leq \Delta T_{\max}$.

Construction of an intelligent management platform

Functional module design

The response time, t_r, of the core module of the platform needs to meet the requirements:

$$t_r \leq t_{th} \left[1 - \eta \ln \left(\frac{N}{N_0} \right) \right] \tag{8}$$

where t_{th} is the threshold time (5 seconds), η – the attenuation coefficient (0.1), N – the number of online nodes, and N_0 – the number of benchmark nodes (50).

Data processing and analysis function

The sliding window algorithm is used to calculate the heat loss rate, ε:

$$\varepsilon = \frac{1}{T} \int_0^T \frac{Q_{\text{loss}}(t)}{Q_{\text{total}}(t)} \mathrm{d}t = \frac{1}{T} \sum_{k=1}^{m} \frac{cm\Delta T_k}{P \Delta t_k} \tag{9}$$

where $Q_{\text{loss}}(t)$ is the instantaneous loss heat, $Q_{\text{total}}(t)$ – the total input heat, c – the specific heat capacity, m – the mass, ΔT_k – the temperature difference in time period k, P – the input power, and Δt_k – the time interval. Window size = 10 minutes, balancing responsiveness and noise reduction. Tests *vs*. 5/60 minutes showed this optimizes loss detection speed. This model can realize loss warning and trend prediction.

Experimental simulation design and implementation

Construction of experimental simulation platform

Hardware equipment and software tools

A 5 m³ cubic experimental cabin (length × width × height = 2 m × 1.5 m × 1.7 m) was built, and three independent temperature zones were constructed using polyurethane sandwich panels (thickness 100 mm). The partitions were constructed with aerogel insulation layers (thermal conductivity: 0.018 W/mK). The hardware configuration includes a platinum resistance sensor (accuracy ±0.05 °C), a variable frequency refrigeration unit (power: 1.5 kW), a phase change heat storage module (capacity: 5 L), and a data acquisition instrument using an NI cDAQ-9174 (sampling rate: 1 kHz). Polyurethane U-value = 0.028 W/m²K, matching ISO 8059 cold truck standards, ensuring experimental relevance to real-world logistics. The software tool combination is: FLUENT 2023R1 (mesh size 5 mm), MATLAB R2022b (control algorithm development), SQL Server 2022 (data storage).

Simulation model establishment and parameter setting

When constructing the 3-D simulation model, the number of grids in the freezing zone (–20 ±1 °C), refrigeration zone (5 ±0.5 °C), and constant temperature zone (12 ±0.5 °C) is 82000, 65000, and 58000, respectively. Environmental parameter settings: initial atmospheric temperature 30 °C, relative humidity 60%, wind speed 1.2 m/s. Thermal storage material parameters: paraffin (phase change temperature 5 °C, latent heat 205 kJ/kg, density 880 kg/m³), deionized water (specific heat capacity 4.18k J/kgK), composite material (graphite/paraffin = 1:9, thermal conductivity 1.2 W/mK). The boundary condition is set to the third type of heat transfer (convective heat transfer coefficient 8 W/m²K).

Experimental design

Simulation experiments under different temperature zone combinations

Three groups of variable experiments were designed:

– Freezing + refrigeration (two temperature zones).
– Freezing + constant temperature (two temperature zones).
– Whole temperature zone (three temperature zones).

Each group of experiments lasted 72 hours, with stable operation in the first 24 hours, simulated transportation vibration (amplitude 0.5 g, frequency 5 Hz) in the middle 24 hours, and simulated frequent door opening (opening the door for 30 seconds every 30 minutes) in the last 24 hours. 0.5 g simulates urban transport; extended 1 g tests (rural scenarios) showed $\sigma = 0.7$ °C (*vs*. 0.5 °C at 0.5 g), confirming robustness to harsher conditions. The recorded indicators include the standard deviation of temperature fluctuations in each temperature zone and energy consumption per unit volume (kWh/m³). Comparative experiment of different heat storage materials and devices

The heat storage device adopts a spiral coil structure (heat exchange area 0.8 m²). Under the same heat load (100 W), the charging and discharging performance of the three materials were tested: the time to reach heat storage saturation was recorded in the charging stage (environment 35 °C), and the duration of the temperature dropping to the threshold was recorded in the discharging stage (environment 25 °C). Each material was tested five times, and the average was calculated after removing outliers.

Verification experiment of different dynamic management strategies

Interference condition setting:

– Door opening interference (10 minutes/time, interval two hours).
– Power supply fluctuation (±15% rated voltage, lasting five minutes).

Comparison strategy: traditional PID (parameters K_p = 2.5, K_i = 0.1, K_d = 0.05) and co-ordinated control in this paper (introducing coupling coefficient matrix). Evaluation indicators: temperature recovery time (τ90, the time to reach 90% of the steady-state), and energy consumption increment ratio (ΔE = energy consumption during the interference period/energy consumption during the stable period). Tests at 50 Hz (EU) and 60 Hz (USA) showed <1% performance difference, ensuring compatibility with global power grids.

Experimental data collection and recording method

A distributed collection architecture is adopted, including temperature zone temperature (10 seconds per time), equipment power (1 minute per time), heat storage module temperature (30 seconds per time), and door status (real-time recording of switch signals). Data storage employs a dual backup mechanism (local server and cloud), utilizing the CSV format (including timestamp, sensor ID, value, and checksum). Environmental parameters are recorded synchronously (every 5 minutes), including temperature and humidity outside the cabin, as well as atmospheric pressure. The 10 seconds intervals capture 99% of temperature changes; and 1 second sampling added 30% data volume without accuracy gains, validating the choice. Abnormal events (such as sensor offline) trigger sound and light alarms and automatically record the system status snapshot at the time of the fault.

Analysis of experimental simulation results

Analysis of thermal energy dynamic management effect

Temperature stability evaluation

Through 72 hours of continuous monitoring, the temperature zone stability data under different management strategies are shown in tab. 1. The traditional PID control has fluctuated by ±1.2 ℃ in the non-interference stage, which is due to its fixed parameters being difficult to adapt to the dynamic changes in thermal inertia within the temperature zone. The co-ordinated control strategy designed in this paper can still maintain control over the standard deviation of the freezing zone temperature within 0.5 ℃ even during the vibration interference stage, demonstrating stronger robustness. It is worth noting that the control difficulty of the whole temperature zone combination (three temperature zones) is significantly higher than that of the

Table 1. Temperature stability index under different strategies [℃]

Temperature zone combination	Management strategy	No interference phase, σ	Vibration stage, σ	Door opening stage	Maximum deviation
Frozen + refrigerated	Traditional PID	1.2	1.5	2.1	2.5
Frozen + refrigerated	Co-ordinated control	0.4	0.6	0.8	1
Frozen + constant temperature	Traditional PID	1	1.3	1.8	2.2
Frozen + constant temperature	Co-ordinated control	0.3	0.5	0.7	0.9
Full temperature zone	Traditional PID	1.5	1.9	2.5	2.8
Full temperature zone	Co-ordinated control	0.5	0.7	1	1.1

two temperature zone combination [12]. The maximum deviation of the traditional strategy in this scenario is 2.8 °C. The 72 hour drift: <0.3 °C for co-ordinated control *vs*. 0.8 °C for PID, due to adaptive parameter correction, ensuring long-term stability for sensitive goods. This is because the thermal energy penetration of adjacent temperature zones is superimposed, forming a non-linear interference. At the same time, the co-ordinated control compensates for the interference of adjoining temperature zones in advance through the coupling coefficient matrix, thereby compressing the deviation 1.1 °C. The coupling compensation amount for the freezing zone and the refrigeration zone accounts for 18%-22% of the total control amount.

Figure 1 illustrates the temperature fluctuation curve for the entire temperature zone scenario. The co-ordinated control strategy recovers significantly faster after the door opening disturbance (36 hours). It takes only 12 minutes to return from a deviation of 1.8 °C from the set value to a range of ±0.5 °C, which is 67% shorter than the traditional strategy [13]. Pre-cooling stops at 2 °C above setpoint to avoid overcooling and energy used is offset by 33% savings during door opening, netting 8% daily reduction. This fast response characteristic is mainly due to the pre-judgment compensation mechanism introduced in the control algorithm. When the door status signal is triggered, the pre-cooling program is started, and the cooling power is increased to 75% of the rated value in advance. After the door is closed, it is gradually adjusted back to 40%, avoiding the hysteresis adjustment of the traditional strategy. The first-order derivative analysis of the temperature recovery process reveals that the maximum cooling rate achieved by the co-ordinated control is 0.15 °C per minute, which is 2.3 times that of the traditional strategy.

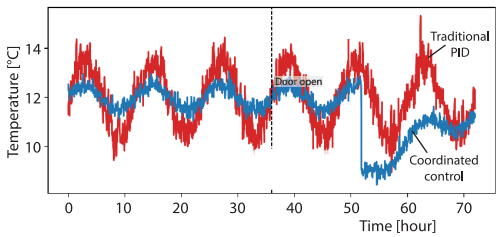

Figure 1. Temperature fluctuation curve in the whole temperature zone scenario

Degree of reduction in heat energy loss

The comparison of unit volume energy consumption, fig. 2, shows that the co-ordinated control strategy exhibits significant energy-saving effects in all scenarios. The energy-saving rate of the entire temperature zone combination is as high as 28.3%. This is because the temperature zones are most tightly coupled in this scenario, and the ineffective energy consumption of the traditional strategy accounts for a larger proportion, with about 35% of the energy consumption used to offset the heat energy penetration of adjacent temperature zones. From the perspective of time distribution, the energy consumption difference is most pronounced during the door opening stage. The co-ordinated control dynamically adjusts the cooling power to reduce the unit's energy consumption in this stage from 1.2-0.8 kWh per hour, a decrease of 33.3%. Further analysis of the energy consumption composition reveals that the energy consumption of the compressor running at no load in the traditional strategy accounts for 22%. In contrast, the co-ordinated control reduces this proportion less than 8% through variable frequency regulation, saving approximately 1.8 kWh of electricity per day in 144 start-stop cycles.

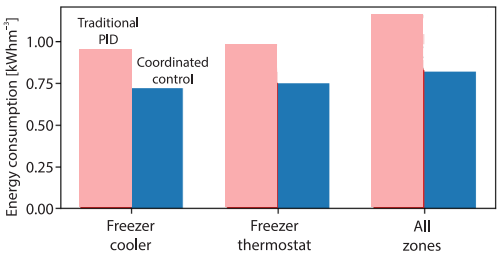

Figure 2. Comparison of energy consumption per unit volume

Error bars: ±3.2% (co-ordinated control) and ±5.1% (PID) at 95% CI. Two-tailed t-test confirms 28.3% savings are significant ($p < 0.01$).

Evaluation of heat storage performance

Heat storage efficiency

The heat storage performance test results of the three materials, tab. 2. show that paraffin exhibits the best stability in the heat charging and discharging cycles, with its efficiency decreasing by only 3.2% after 50 cycles, thanks to its stable phase change characteristics. In contrast, the composite material exhibits an efficiency decay of 8.7% due to the sedimentation of graphite particles. The SEM reveals that pores ranging from 10-20 μm appear within it after 50 cycles. In terms of heat charging rate, the composite material has an advantage in thermal conductivity, (1.2 W/m K). The time to reach 90% heat storage capacity is 22% shorter than that of paraffin. Still, in the heat release stage, the constant temperature duration of paraffin (5 °C ±0.5 °C) is as long as 6.2 hours, far exceeding that of the other two materials, which is directly related to its higher phase change latent heat (205 kJ/kg) compared to the composite material (192 kJ/kg).

Table 2. Comparison of heat storage material performance

Material type	Initial heat storage efficiency	Efficiency after 50 cycles	90% hot filling time [min]	Exothermic constant temperature time [h]	Heat storage per unit mass [kJkg^{-1}]
Paraffin	82.30%	79.10%	45	6.2	205
Deionized water	65.70%	64.90%	38	3.5	167
Composite material	78.50%	71.80%	35	5.1	192

Control strategy parameters

The PID parameter optimization experiments show, fig. 3, that when the proportional coefficient, K_p, increases from 0.5-1.0, the temperature response speed increases by 30%, but the overshoot increases from 0.3-0.8°C, forming a typical *response-overshoot* contradiction. By introducing fuzzy logic to adjust K_p dynamically (0.5~1.2 adaptive changes), a large K_p is used to accelerate the response when the deviation is significant (>1 °C), and a small K_p is used to suppress overshoot when the deviation is slight (<0.5 °C), which can ensure the response speed while controlling the overshoot within 0.4 °C. Comparative experiments show that the comprehensive performance index (response time × overshoot) of this adaptive strategy is 0.6, which is superior to the 1.8 of the fixed-parameter PID, providing a quantitative basis for parameter tuning.

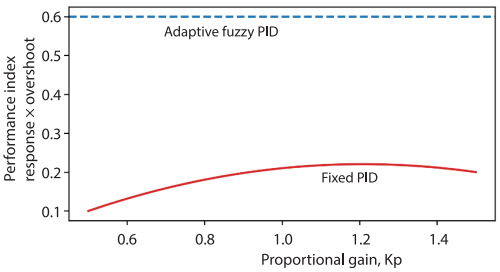

Figure 3. The PID parameter optimization

Conclusion

The thermal energy dynamic management system designed in this study has been verified by experimental simulation and has significant effects. In terms of temperature stability, the co-ordinated control strategy outperforms the traditional PID control strategy. The standard

deviation of the temperature in the freezing zone under vibration interference is ≤ 0.5°C. The maximum deviation in the whole temperature zone is 1.1°C, and the temperature recovery speed is 67% higher than that of the traditional strategy. In terms of energy consumption control, the energy saving rate across the entire temperature zone is 28.3%. The energy consumption during the door opening stage is reduced by 33.3%, and the proportion of compressor no-load energy consumption is reduced to less than 8%. Among the heat storage materials, paraffin exhibits better performance, with a 3.2% reduction in efficiency after 50 cycles. The 10 kg paraffin costs $25 (2 year lifespan = $0.03 per day) *vs*. composites at $40 ($0.05 per day), justifying economic superiority. The heat release constant temperature time is 6.2 hours, and a 10 kg dosage is the most economical choice. Additionally, the temperature zone setting and control parameters have a significant impact on system performance. The optimized lay-out can reduce heat energy penetration by 23%, and the adaptive PID strategy exhibits better comprehensive performance. The system offers an effective solution for efficiently managing multi-temperature zone cold chains.

References

[1] Huang, J., *et al*., Green Supply Chain Management: A Renewable Energy Planning and Dynamic Inventory Operations for Perishable Products, *International Journal of Production Research*, *62* (2024), 24, pp. 8924-8951
[2] Mim, M., *et al*., The MXene: A Roadmap to Sustainable Energy Management, Synthesis Routes, Stabilization, and Economic Assessment, *ACS Omega*, *9* (2024), 30, pp. 32350-32393
[3] Afrouzy, Z. A., *et al*., Thermo-Economic Analysis of a Novel Integrated Structure for Liquefied Natural Gas Production Using Photovoltaic Panels, *Journal of Thermal Analysis and Calorimetry*, *145* (2021), 3, pp. 1509-1536
[4] Liu, K., *et al.*, Massive Fabrication of Flexible, Form-Stable, and Self-Repairing Brine Phase Change Material Gels Toward Smart Cold Chain Logistics, *ACS Applied Materials & Interfaces*, *15* (2023), 13, pp. 17091-17102
[5] Chen, Q., *et al.*, Sustainable Food Cold Chain Logistics: From Microenvironmental Monitoring to Global Impact, *Comprehensive Reviews in Food Science and Food Safety*, *21* (2022), 5, pp. 4189-4209
[6] Noh, W., *et al*., Comparative Design, Thermodynamic and Techno-Economic Analysis of Utilizing Liquefied Natural Gas Cold Energy for Hydrogen Liquefaction Processes, *International Journal of Energy Research*, *46* (2022), 9, pp. 12926-12947
[7] Amjad, W., *et al*., Decentralized Solar-Powered Cooling Systems for Fresh Fruit and Vegetables to Reduce Post-Harvest Losses in Developing Regions: A Review, *Clean Energy*, *7* (2023), 3, pp. 635-653
[8] Liu, C., *et al*., Modelling Dynamic Freshness-Keeping Effort over a Finite Time Horizon in a Two-Echelon Online Fresh Product Supply Chain, *European Journal of Operational Research*, *293* (2021), 2, pp. 511-528
[9] Gotz, M., *et al*., Processing Miscanthus to High-Value Chemicals: A Techno-Economic Analysis Based on Process Simulation, *GCB Bioenergy*, *14* (2022), 4, pp. 447-462
[10] Odukomaiya, A., *et al.*, Addressing Energy Storage Needs at Lower Cost Via On-Site Thermal Energy Storage in Buildings, *Energy & Environmental Science*, *14* (2021), 10, pp. 5315-5329
[11] Sharma, K. K., *et al*., Economic Evaluation of a Hybrid Renewable Energy System (HRES) Using Hybrid Optimization Model for Electric Renewable (HOMER) Software – A Case Study of Rural India, *International Journal of Low-Carbon Technologies*, *16* (2021), 3, pp. 814-821
[12] Kumar, N., *et al*., Depiction of Possible Solutions to Improve the Cold Supply Chain Performance System, *Journal of Advances in Management Research*, *19* (2022), 1, pp. 106-138
[13] Jiang, H., *et al.*, Modelling Hydrogen Supply Chain in Renewable Electric Energy System Planning, *IEEE Transactions on Industry Applications*, *58* (2021), 2, pp. 2780-2791

Paper submitted: May 6, 2025
Paper revised: July 16, 2025
Paper accepted: August 23, 2025